



International Symposium on Imaging, Sensing, and Optical Memory (ISOM '19), Niigata, Japan

Simulation on near-field light on recording medium generated by semiconductor ring resonator with metal nano-antenna for heat-assisted magnetic recording

Ryuichi Katayama¹ · Satoshi Sugiura²

Received: 25 February 2020 / Accepted: 30 July 2020 / Published online: 20 August 2020
© The Optical Society of Japan 2020

Abstract

Heat-assisted magnetic recording (HAMR) is a promising technology for achieving more than 10 Tbit/inch² recording density. A near-field transducer (NFT), which forms a small light spot on a recording medium, is necessary in HAMR. However, the heat generated by the NFT would melt the NFT itself. To solve this problem, the authors have proposed a novel device, in which a metal nano-antenna is attached to a semiconductor ring resonator. In this paper, the near-field light generated by this device was analyzed through a numerical simulation based on a 3-dimensional model including the recording medium to optimize the structure of the device. It was found that how to excite a desired eigenmode selectively among some eigenmodes is important to make the device effective. A light spot with a diameter of about 25 nm, which corresponds to the recording density of 1 Tb/inch², was obtained on the surface of the recording medium. It was also found that the design parameters of the device must be optimized considering the recording medium.

Keywords Heat-assisted magnetic recording · Near-field light · Ring resonator · Nano-antenna · Recording medium · Numerical simulation

1 Introduction

In the present information explosion era, there is a prediction that the amount of the data produced all over the world will reach 40 ZB in 2025. Therefore, in hard disk drives, which play an important role in online storage systems, the demand for higher recording density is growing daily. The recording density of hard disk drives is increasing by 30%/year and has reached 816 Gbit/inch² in 2016. However, to further increase the recording density, the “trilemma” among signal-to-noise ratio, thermal stability, and recordability needs to be solved [1]. To secure the signal-to-noise ratio for a smaller

recorded mark, it is necessary to make the magnetic grain size of the recording medium smaller, thereby increasing the thermal fluctuation and making the recorded mark unstable. To record a smaller mark stably, the recording medium must have a higher coercivity, thereby requiring a higher magnetic field intensity for recording, which is difficult to obtain using a conventional magnetic recording head. To overcome this difficulty and to achieve a recording density of more than 10 Tbit/inch², a novel technology must be introduced. Heat-assisted magnetic recording (HAMR) [2–6], microwave-assisted magnetic recording (MAMR) [7–11], two-dimensional magnetic recording (TDMR) [12–16], and bit-patterned media (BPM) [17–21] are promising technologies for this purpose. Among them, HAMR is the closest to practical use and a recording density of 1 Tbit/inch² has already been demonstrated [6]. In HAMR, the recording medium is heated locally by a light spot smaller than the diffraction limit to reduce the coercivity and to enable the mark to be recorded using the conventional magnetic recording head. Therefore, a near-field transducer (NFT), which

✉ Ryuichi Katayama
r-katayama@fit.ac.jp

¹ Department of Information Electronics, Faculty of Engineering, Fukuoka Institute of Technology, 3-30-1, Wajiro-higashi, Higashi-ku, Fukuoka 811-0295, Japan

² InnovaStella, Inc., 465 Ohsato-cho, Kofu, Yamanashi 400-0053, Japan

forms such a light spot with the order of 10 nm in diameter on the recording medium, is necessary, and various types of NFT, such as lollipop [4], E-antenna [5], and beaked plate [22] types, were previously proposed. However, these NFTs have a problem that the heat generated by the NFT would melt the NFT itself when the recording density becomes higher and the size of the light spot becomes smaller. This is because the NFT and the light source are separated and extra heat is caused by the optical loss between them. Moreover, the overall size of the device including the NFT and the light source becomes large.

To solve this problem, Kuriyama et al. proposed a novel mesa-type device for a HAMR heat source [23]. One of the authors analyzed the near-field light generated by the mesa-type device through a numerical simulation [24–26]. Based on this concept, the authors have proposed a novel ring-resonator-type device for a HAMR heat source [27]. Figure 1 shows the structure of the ring-resonator-type device. In this device, a metal nano-antenna, which acts as the NFT, is attached to a semiconductor ring resonator containing quantum dots [28, 29], which acts as a light source. In both the mesa-type and the ring-resonator-type devices, extra heat caused by the optical loss can be minimized, because the NFT and the light source are integrated, and the overall size of the device becomes small. Moreover, the ring-resonator-type device is superior to the mesa-type device in some respects. First, more optical energy is provided for the nano-antenna, because the nano-antenna is placed adjacent to the active layer of the ring resonator. Second, the ring resonator is excited by electric current, which is more practical. Third, the manufacturing process has higher affinity with that of the magnetic recording head because the stacking direction is parallel to that of the magnetic recording head. The authors have analyzed the near-field light generated by the ring-resonator-type device through a numerical simulation based on a 2-dimensional model [27] and a 3-dimensional model [30]. However, the recording medium has not been considered in the previous studies, although the role of the nano-antenna is to provide the optical energy for a small region on the recording medium. The objective of this study is to conduct

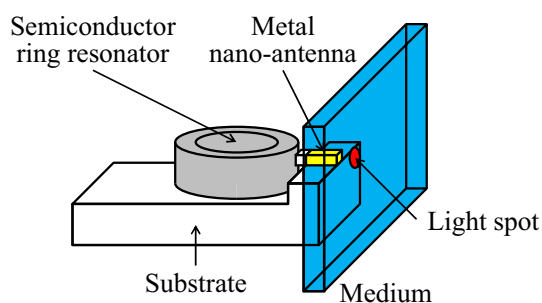


Fig. 1 Structure of proposed device

a more practical simulation for a model including the recording medium to optimize the structure of the device.

2 Simulation methods

Figure 2 shows the simulation model. A metal nano-antenna is attached to the side surface of a semiconductor ring resonator via a dielectric spacer. The ring resonator contains an active layer sandwiched between two cladding layers. The nano-antenna and the ring resonator are formed on a certain semiconductor substrate, which is not shown in the figure. Two electrodes are formed on the top of the upper cladding layer and on the bottom of the lower cladding layer, which are not shown in the figure either. If an electric current is injected to the active layer through the electrodes, the ring resonator acts as a ring laser [31–34] and generates light. The light is directly provided to the nano-antenna and a near-field light is generated at the tip (right end) of the nano-antenna. The recording medium is placed in close proximity to the nano-antenna across a narrow gap. The recording medium consists of a recording layer, an underlayer, a heat-sink layer, and a substrate [35]. The recording layer is made of a magnetic material and marks are recorded in this layer. The underlayer makes the recording layer perpendicularly magnetized. The heatsink layer helps the heat generated by the near-field light escape from the recording layer. A Cartesian coordinate was set as shown in the figure. The x - y plane was defined parallel to the active layer, where the x - and y -axes were parallel and perpendicular to the nano-antenna, respectively, and the z -axis was defined perpendicular to the active layer.

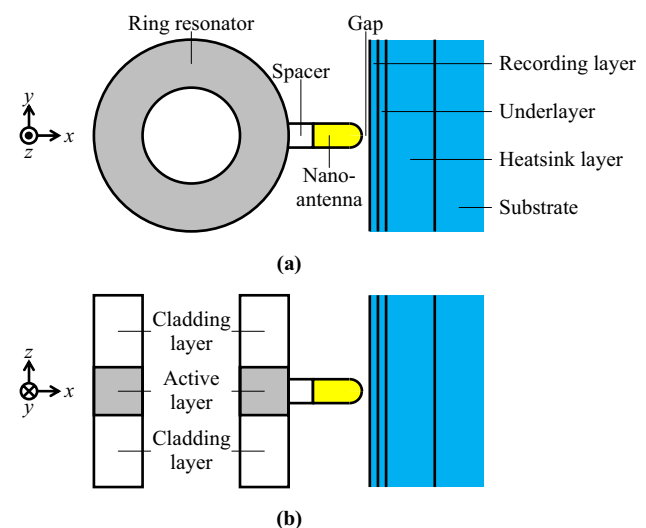


Fig. 2 Simulation model: (a) plane view and (b) side view

The device has some eigenmodes. The resonance wavelength and the electric field intensity distribution for each eigenmode were numerically simulated. The materials and the refractive indices of the device and the recording medium used in the simulation are shown in Table 1. The dimensions of the device and the recording medium used in the simulation are shown in Table 2. The inner and outer diameters of the ring resonator were smaller than those in the practical case to reduce the number of the eigenmodes and to make the analysis easier. The length of the nano-antenna and the thickness of the spacer were varied later. The oscillating wavelength range of the ring resonator when it acts as a ring laser was 1000–1100 nm, assuming that the active layer contains InAs quantum dots that have a gain around 1050 nm. The 3-dimensional finite element method [36] was used in the simulation. Because the model was symmetric with respect to the x - z and x - y planes, the calculation region was reduced to a quarter in which both y and z were positive. The actual calculation was conducted using the COMSOL Multiphysics software according to the following steps: first, the parameters shown in Tables 1 and 2 and the calculation region were defined. Next, a quarter of the model shown in Fig. 2 was constructed using these parameters. Next, the boundary conditions were set, where the x - z and x - y planes were magnetic walls. Next, a mesh structure was generated, where the mesh size was smaller as the refractive index of the material was higher. Finally, the eigenmode analysis was conducted to calculate the resonance wavelengths and their corresponding electric field intensity distributions within the specified wavelength range.

3 Simulation results

First, the relationship between the eigenmodes of the device and the near-field light was investigated. It was found that the device had three eigenmodes, which were named Modes A, B, and C. Table 3 shows the calculated resonance wavelength and order of mode for each eigenmode. The

Table 1 Materials and refractive indices of device and medium

	Material	Refractive index
Active layer	GaAs	3.5
Cladding layers	AlGaAs	3.1
Nano-antenna	Au	$0.28 + 7.2i$
Spacer	SiO ₂	1.5
Surrounding region	Air	1.0
Recording layer	FePt	$2.9 + 1.5i$
Underlayer	MgO	1.7
Heatsink layer	Cr	$0.26 + 5.3i$
Substrate	Glass	1.5

Table 2 Dimensions of device and medium

	Dimension (nm)
Inner diameter of ring resonator	1000
Outer diameter of ring resonator	2000
Thickness of active layer	200
Diameter of nano-antenna	50
Length of nano-antenna	100 (varied later)
Thickness of spacer	50 (varied later)
Thickness of recording layer	10
Thickness of underlayer	15
Thickness of heatsink layer	100
Gap between nano-antenna and medium	5

resonance wavelengths were different among the eigenmodes. Each eigenmode was a single mode in the vertical and radial directions and a whispering gallery mode in the tangential direction. Figures 3, 4 and 5 show the calculated electric field intensity distributions for Modes A, B, and C, respectively. The distributions in the x - y and x - z planes are shown in Figs. 3a, 4a and 5a and Figs. 3b, 4b and 5b, respectively, and their enlarged views around the nano-antenna are shown in Figs. 3c, 4c and 5c and Figs. 3d, 4d and 5d, respectively. The calculation region was $-1500 \text{ nm} < x < 1780 \text{ nm}$, $0 \text{ nm} < y < 1500 \text{ nm}$, and $0 \text{ nm} < z < 1500 \text{ nm}$. Therefore, only the regions in which y is positive are shown in Figs. 3a, 4a and 5a and Figs. 3c, 4c and 5c, and only the regions in which z is positive are shown in Figs. 3b, 4b and 5b and Figs. 3d, 4d and 5d. In each figure, the electric field intensity is high in the red area and low in the blue area. In Modes A and C, no near-field light was observed between the tip of the nano-antenna and the surface of the recording medium. On the other hand, in Mode B, a certain amount of near-field light was observed between the tip of the nano-antenna and the surface of the recording medium. Moreover, the directions of the electric field are represented as red arrows in Figs. 3a, 4a and 5a and Figs. 3b, 4b and 5b. In Modes A and C, the direction of the electric field in the ring resonator was nearly vertical, that is, Modes A and C were transverse-magnetic-like (TM-like) mode. On the other hand, in Mode B, the direction of the electric field in the ring resonator was nearly radial, that is, Mode B was transverse-electric-like (TE-like) mode.

Table 3 Calculated resonance wavelengths and orders of mode

Mode	Resonance wavelength (nm)	Order of mode		
		Vertical	Radial	Tangential
Mode A	1082.4	0	1	15
Mode B	1041.1	0	1	15
Mode C	1026.0	0	1	16

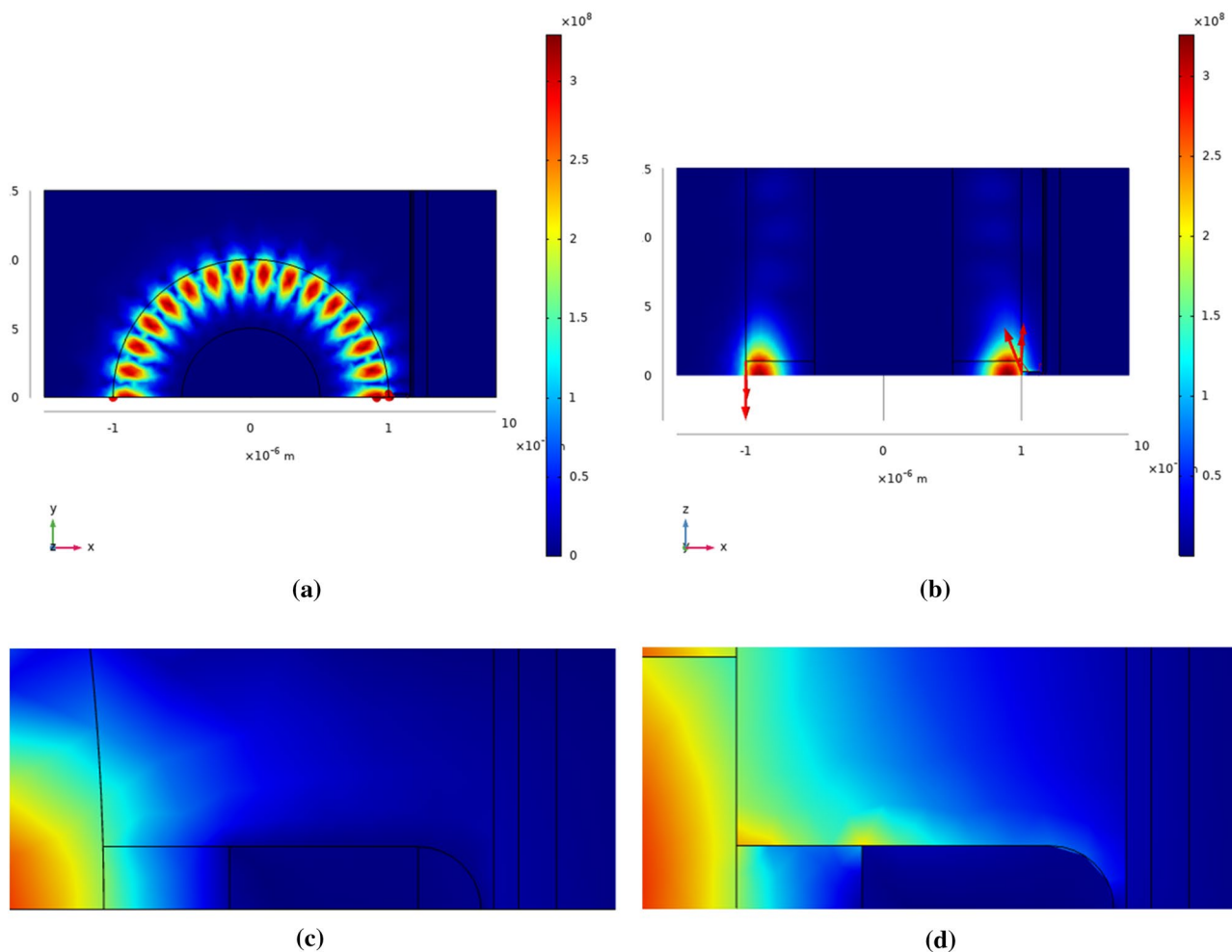


Fig. 3 Calculated electric field intensity distribution for Mode A: **(a)** x - y plane, **(b)** x - z plane, **(c)** enlarged view of **(a)** around nano-antenna, and **(d)** enlarged view of **(b)** around nano-antenna

Next, the near-field light on the surface of the recording medium was investigated for Mode B. Figures 6a and 6b show the calculated electric field intensity distribution on the surface of the recording medium along the y - and z -directions, respectively. In each figure, the horizontal axis indicates the position in each direction while the vertical axis indicates the relative electric field intensity. Here, the light intensity distribution is given by the square of the electric field intensity distribution. If the diameter of the light spot formed on the recording medium is defined as the full width at half maximum of the light intensity distribution, the diameter was about 25 nm in both the y - and z -directions.

Next, the relationship between the length of the nano-antenna and the near-field light was investigated for Mode B. Figure 7 shows the calculated dependence of the peak electric field intensity on the length of the nano-antenna, when the thickness of the spacer was fixed to 50 nm. The horizontal axis indicates the length of the nano-antenna while the vertical axis indicates the electric field intensity

at $y=0$ nm and $z=0$ nm. The length of the nano-antenna was varied from 50 to 400 nm. The blue and red lines represent the electric field intensities at the tip of the nano-antenna and on the surface of the recording medium, respectively. It was found that the electric field intensity and the light intensity on the surface of the recording medium were about 75% and 56% of those at the tip of the nano-antenna, respectively. Although the electric field intensity changed with the length of the nano-antenna rather irregularly, it was found that the optimum length of the nano-antenna was about 150 nm.

Next, the relationship between the thickness of the spacer and the near-field light was investigated for Mode B. Figure 8 shows the calculated dependence of the peak electric field intensity on the thickness of the spacer, when the length of the nano-antenna was fixed to 100 nm. The horizontal axis indicates the thickness of the spacer while the vertical axis indicates the electric field intensity at $y=0$ nm and $z=0$ nm. The thickness of the spacer was varied from 12.5 to 100 nm. The blue and red lines represent the electric field

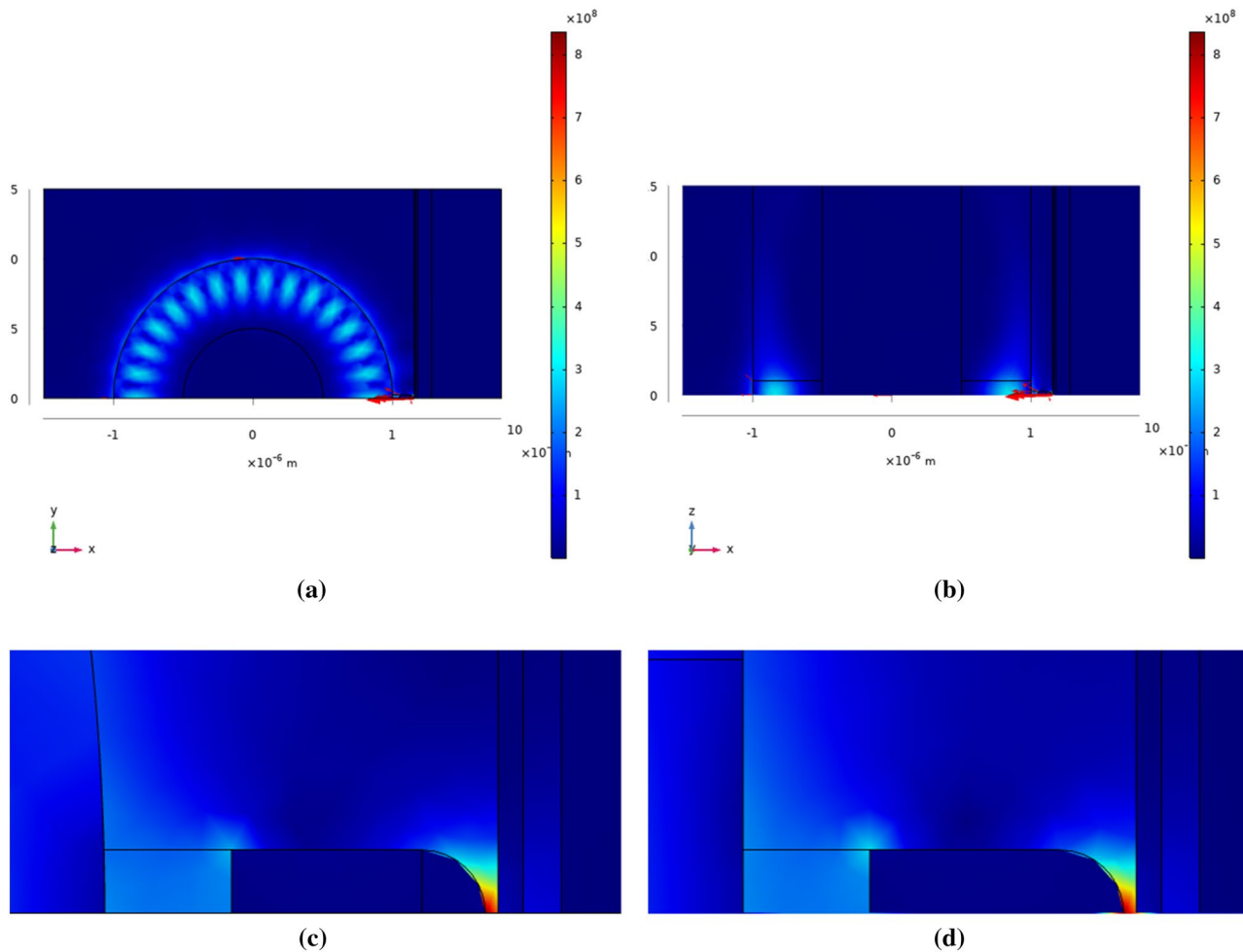


Fig. 4 Calculated electric field intensity distribution for Mode B: **(a)** x - y plane, **(b)** x - z plane, **(c)** enlarged view of **(a)** around nano-antenna, and **(d)** enlarged view of **(b)** around nano-antenna

intensities at the tip of the nano-antenna and on the surface of the recording medium, respectively. Again, it was found that the electric field intensity and the light intensity on the surface of the recording medium were about 75% and 56% of those at the tip of the nano-antenna, respectively. Although the electric field intensity changed with the thickness of the spacer rather irregularly, it was found that the optimum thickness of the spacer was less than 25 nm.

4 Discussion

First, the relationship between the eigenmodes of the device and the near-field light is discussed. In Modes A and C, as described in Sect. 3, the direction of the electric field in the ring resonator was nearly vertical, which was perpendicular to the nano-antenna. In this case, the electric field does not induce electric dipoles in the nano-antenna along the x -axis. Therefore, no near-field light was generated at the

tip of the nano-antenna. On the other hand, in Mode B, as described in Sect. 3, the direction of the electric field in the ring resonator was nearly radial, which was parallel to the nano-antenna. In this case, the electric field induces electric dipoles in the nano-antenna along the x -axis. Therefore, a certain amount of near-field light was generated at the tip of the nano-antenna. From these results, it can be concluded that how to excite Mode B selectively is important to make the device effective. As shown in Figs. 3b, 4b and 5b, the electric field was more strongly confined to the active layer in the vertical direction in Mode B than in Modes A and C. This means that the gain for laser oscillation is higher for Mode B than for Modes A and C without the nano-antenna. However, the nano-antenna increases the loss for laser oscillation for Mode B. The balance between the gain and loss determines the eigenmode to be excited.

Next, the near-field light on the surface of the recording medium was discussed. As described in Sect. 3, the diameter of the light spot formed on the recording medium was

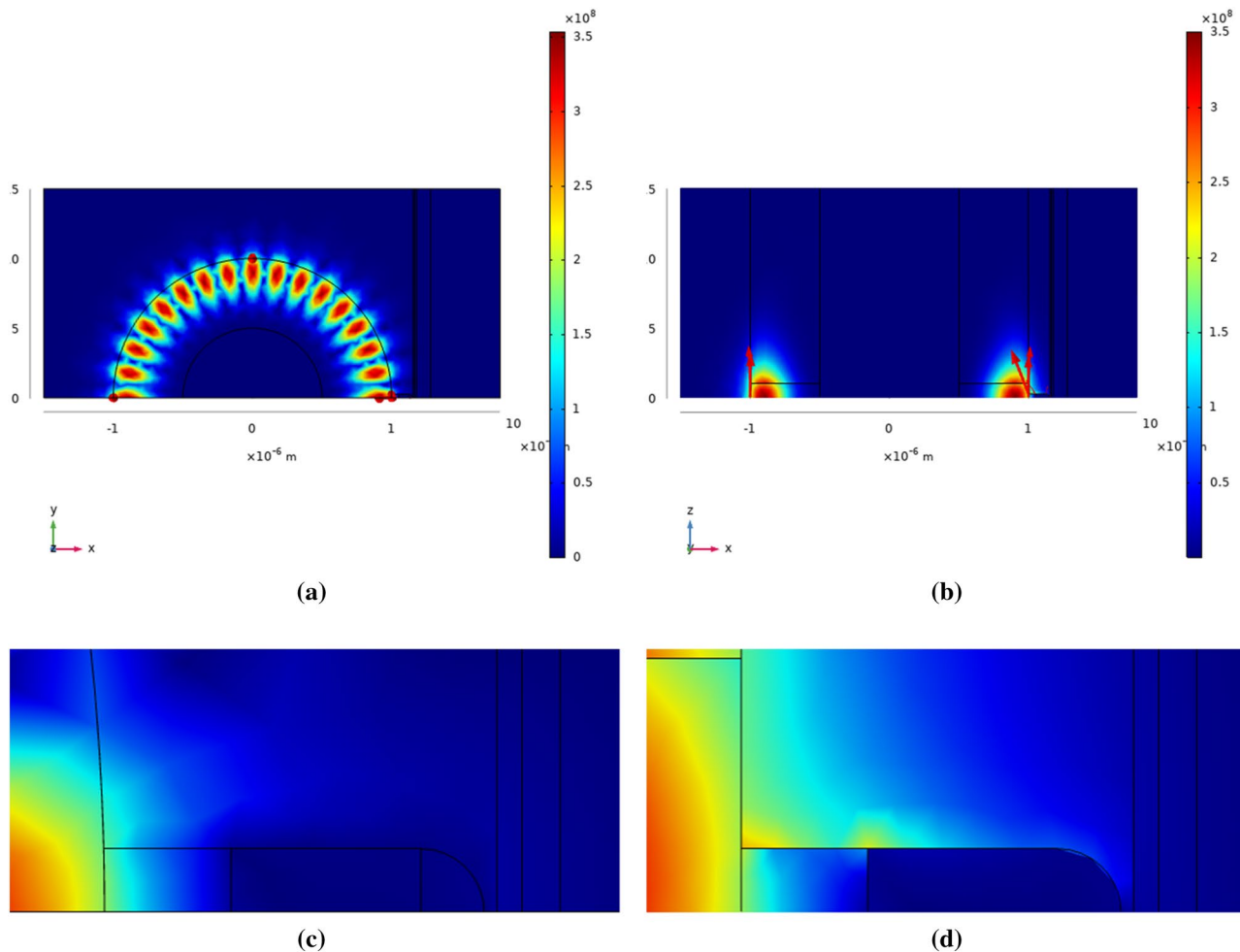


Fig. 5 Calculated electric field intensity distribution for Mode C: **(a)** x - y plane, **(b)** x - z plane, **(c)** enlarged view of **(a)** around nano-antenna, and **(d)** enlarged view of **(b)** around nano-antenna

about 25 nm, which was much smaller than the diameter of the nano-antenna. In this simulation, the refractive index of the recording layer was a fixed value. However, in the actual HAMR, it changes depending on the temperature. Therefore, the effect of the refractive index change on the electric field intensity distribution on the recording layer was investigated. Generally, the refractive index of a material decreases with the temperature rise mainly due to thermal expansion. Among several materials, the dependence of the refractive index of Au and Ag on the temperature is reported in Ref. [37]. Here, the maximum temperature rise of the recording layer was assumed to be 500 deg. considering its Curie temperature. According to Ref. [37], the refractive index decrease of Au and Ag with the temperature rise of 500 deg. was calculated to be about 8% and 20%, respectively. Since the thermal expansion coefficients of Fe and Pt, which are the materials of the recording layer, are smaller than those of Au and Ag, the refractive index decrease of the recording layer with the temperature rise of 500 deg. was

considered to be less than 8%. Based on this consideration, the electric field intensity distribution on the recording layer was calculated when the refractive index of the recording layer decreased by 5–10% within the center portion of the light spot (5–20 nm in diameter). The result showed that the change in the diameter of the light spot due to the refractive index change was negligible. In the actual HAMR, the size of the recorded mark is determined not only by the diameter of the light spot but also by the magnetic grain size of the recording layer. The effect of the magnetic grain size might be larger than that of the change in the diameter of the light spot. If the area of the light spot is assumed to be the area of one bit, the diameter of 25 nm corresponds to the recording density of 1.0 Tb/inch². This means that the feasibility of the recording density of 1 Tb/inch² was confirmed. To further increase the recording density, it is necessary to decrease the diameter of the nano-antenna.

Next, the relationship between the design parameters of the device (the length of the nano-antenna and the thickness

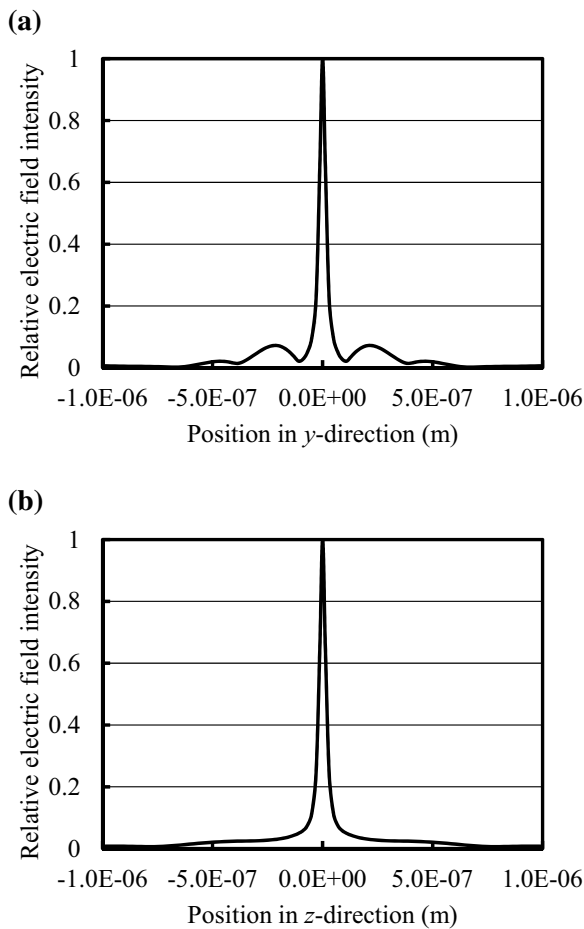


Fig. 6 Calculated electric field intensity distribution on medium surface: (a) y-direction and (b) z-direction

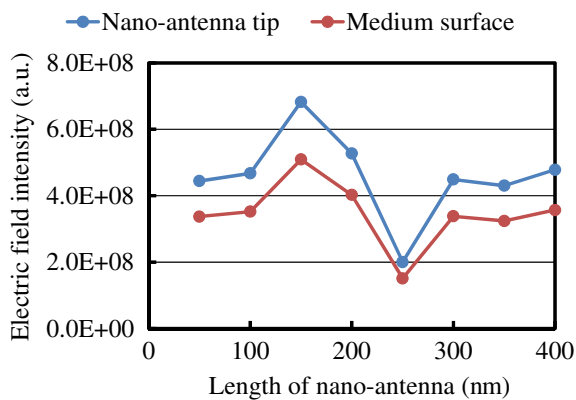


Fig. 7 Calculated dependence of peak electric field intensity on length of nano-antenna

of the spacer) and the near-field light is discussed. As described in Sect. 3, the intensity of the near-field light changed with the design parameters rather irregularly with

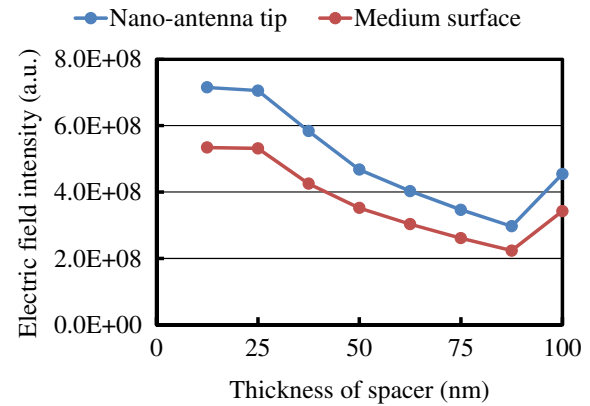


Fig. 8 Calculated dependence of peak electric field intensity on thickness of spacer

the recording medium. Moreover, the optimum length of the nano-antenna was about 150 nm and the optimum thickness of the spacer was less than 25 nm with the recording medium. On the other hand, according to Ref. [30], the intensity of the near-field light changed with the design parameters rather regularly without the recording medium. Moreover, the optimum length of the nano-antenna was about 200 nm and the optimum thickness of the spacer was less than 25 nm without the recording medium. These results imply that there is some interaction between the nano-antenna and the recording medium that changes the relationship between the design parameters of the device and the near-field light. Therefore, it can be concluded that the design parameters of the device must be optimized considering the recording medium.

Next, the light power necessary for the actual HAMR is discussed. According to Ref. [23], in which the mesa-type device is described, the thermal impedance of the recording medium was 2500 deg/mW when the diameter of the near-field light spot was 40 nm. Moreover, the light power efficiency from the light source to the near-field light spot for the mesa-type device was 0.3%. Although the light power efficiency for the ring-resonator-type device has not been calculated yet, the same order as that for the mesa-type device is expected after the optimization of the device structure because both types have the same concept. In addition, the thermal impedance of the recording medium would increase if the diameter of the near-field light spot would decrease to 25 nm. Consequently, the light power at the light source necessary for achieving a 500 deg temperature rise on the recording medium is estimated to be several tens of mW, which is considered to be feasible.

In this study, as described in Sect. 2, the inner and outer diameters of the ring resonator were rather small to reduce the number of the eigenmodes and to make the analysis easier. However, in the practical case, they must be much larger

so that wires can be bonded to the electrodes formed on the top and bottom of the cladding layers. In this case, the number of the eigenmodes will drastically increase. Many eigenmodes having different wavelengths and different orders of mode in the radial and tangential directions will be excited simultaneously, which will make the device inefficient and unstable. Future work includes a further improvement of the structure of the device so that only a desired eigenmode will be excited selectively even in such a practical case.

5 Conclusions

In this study, the near-field light generated by the ring-resonator-type device for a HAMR heat source, in which a metal nano-antenna is attached to a semiconductor ring resonator, was analyzed through a numerical simulation based on a 3-dimensional model including the recording medium. The device had three eigenmodes. A certain amount of the near-field light was observed between the tip of the nano-antenna and the surface of the recording medium for TE-like mode, but no near-field light was observed there for TM-like mode. Therefore, how to excite TE-like mode selectively is important to make the device effective. A light spot with a diameter of about 25 nm was obtained on the surface of the recording medium, and the feasibility of the recording density of 1 Tb/inch² was confirmed. The intensity of the near-field light changed with the design parameters of the device such as the length of the nano-antenna and the thickness of the spacer rather irregularly with the recording medium. Therefore, the design parameters of the device must be optimized considering the recording medium. As a result, the optimum length of the nano-antenna was about 150 nm and the optimum thickness of the spacer was less than 25 nm. Future work includes a further improvement of the structure of the device in more practical case.

Acknowledgements This work was supported by JSPS KAKENHI Grant number JP19K04541.

References

- Weller, D., Moser, A.: Thermal effect limits in ultrahigh-density magnetic recording. *IEEE Trans. Magn.* **35**, 4423 (1999)
- Saga, H., Nemoto, H., Sukeda, H., Takahashi, M.: New recording method combining thermo-magnetic writing and flux detection. *Jpn. J. Appl. Phys.* **38**, 1839 (1999)
- Kryder, M.H., Gage, E.C., McDaniel, T.W., Challener, W.A., Rottmayer, R.E., Ju, G., Hsia, Y.-T., Erden, M.F.: Heat assisted magnetic recording. *Proc. IEEE* **96**, 1810 (2008)
- Challener, W.A., Peng, C., Itagi, A.V., Karns, D., Peng, W., Peng, Y., Yang, X., Zhu, X., Gokemeijer, N.J., Hsia, Y.-T., Ju, G., Rottmayer, R.E., Seigler, M.A., Gage, E.C.: Heat-assisted magnetic recording by a near-field transducer with efficient optical energy transfer. *Nat. Photonics* **3**, 220 (2009)
- Stipe, B.C., Strand, T.C., Poon, C.C., Balamane, H., Boone, T.D., Katine, J.A., Li, J.-L., Rawat, V., Nemoto, H., Hirotsune, A., Hellwig, O., Ruiz, R., Dobisz, E., Kercher, D.S., Robertson, N., Albrecht, T.R., Terris, B.D.: Magnetic recording at 1.5 Pb m⁻² using an integrated plasmonic antenna. *Nat. Photonics* **4**, 484 (2010)
- Wu, A.Q., Kubota, Y., Klemmer, T., Rausch, T., Peng, C., Peng, Y., Karns, D., Zhu, X., Ding, Y., Chang, E.K.C., Zhao, Y., Zhou, H., Gao, K., Thiele, J.-U., Seigler, M., Ju, G., Gage, E.: HAMR areal density demonstration of 1+ Tbps on spindisk. *IEEE Trans. Magn.* **49**, 779 (2013)
- Thirion, C., Wernsdorfer, W., Maily, D.: Switching of magnetization by nonlinear resonance studied in single nanoparticles. *Nat. Mater.* **2**, 524 (2003)
- Nozaki, Y., Ohta, M., Tateishi, S., Yoshimura, S., Matsuyama, K.: Magnetic force microscopy study of microwave-assisted magnetization reversal in submicron-scale ferromagnetic particles. *Appl. Phys. Lett.* **91**, 082510 (2007)
- Woltersdorf, G., Back, C.H.: Microwave assisted switching of single domain Ni₈₀Fe₂₀ elements. *Phys. Rev. Lett.* **99**, 227207 (2007)
- Zhu, J.G., Zhu, X., Tang, Y.: Microwave assisted magnetic recording. *IEEE Trans. Magn.* **44**, 125 (2008)
- Okamoto, S., Kikuchi, N., Kitakami, O.: Magnetization switching behavior with microwave assistance. *Appl. Phys. Lett.* **93**, 102506 (2008)
- Wood, R., Williams, M., Kavcic, A., Miles, J.: The feasibility of magnetic recording at 10 terabits per square inch on conventional media. *IEEE Trans. Magn.* **45**, 917 (2009)
- Greaves, S., Kanai, Y., Muraoka, H.: Shingled recording for 2–3 Tbit/in². *IEEE Trans. Magn.* **45**, 3823 (2009)
- Krishnan, A.R., Radhakrishnan, R., Vasic, B., Kavcic, A., Ryan, W., Erden, F.: 2-D magnetic recording: read channel modeling and detection. *IEEE Trans. Magn.* **45**, 3830 (2009)
- Chan, K.S., Miles, J.J., Hwang, E., VijayaKumar, B.V.K., Zhu, J.-G., Lin, W.-C., Negi, R.: TDMR platform simulations and experiments. *IEEE Trans. Magn.* **45**, 3837 (2009)
- Victoria, R.H., Morgan, S.M., Momsen, K., Cho, E., Erden, M.F.: Two-dimensional magnetic recording at 10 Tbits/in². *IEEE Trans. Magn.* **48**, 1697 (2012)
- Chou, S.Y., Krauss, P.R., Kong, L.: Nanolithographically defined magnetic structures and quantum magnetic disk. *J. Appl. Phys.* **79**, 6101 (1996)
- Albrecht, M., Rettner, C.T., Moser, A., Best, M.E., Terris, B.D.: Recording performance of high-density patterned perpendicular magnetic media. *Appl. Phys. Lett.* **81**, 2875 (2002)
- Terris, B.D., Thomson, T.: Nanofabricated and self-assembled magnetic structures as data storage media. *J. Phys. D* **38**, R199 (2005)
- Richter, H.J., Dobin, A.Y., Lynch, R.T., Weller, D., Brockie, R.M., Heinonen, O., Gao, K.Z., Xue, J., Veerdonk, R.J.M., Asselin, P., Erden, M.F.: Recording potential of bit-patterned media. *Appl. Phys. Lett.* **88**, 222512 (2006)
- Schabes, M.E.: Micromagnetic simulations for terabit/in² head/media systems. *J. Magn. Mater.* **320**, 2880 (2008)
- Matsumoto, T., Anzai, Y., Shintani, T., Nakamura, K., Nishida, T.: Writing 40 nm marks by using a beaked metallic plate near-field optical probe. *Opt. Lett.* **31**, 259 (2006)
- Kuriyama, K., Chabalko, M.J., Kong, Y., Luo, Y., Schlesinger, T.E., Bain, J.A.: Modeling of polarization effects in Au nanodots excited with InAs quantum dot emitters for use as a HAMR heat source. *IEEE Trans. Magn.* **49**, 3560 (2013)
- Katayama, R.: Simulation on near-field light generated by Au nano-dot on GaAs substrate for heat assisted magnetic recording heat source. *J. Appl. Phys.* **115**, 17B728 (2014)
- Katayama, R.: Simulation on near-field light generated by metal nano-dot on GaAs substrate for heat source of heat-assisted magnetic recording. *Opt. Rev.* **21**, 568 (2014)

26. Katayama, R., Kasuya, T., Sugiura, S., Yoshizawa, K.: Enhancement of near-field light generated by metal nanodot on semiconductor substrate for heat-assisted magnetic recording heat source. *Jpn. J. Appl. Phys.* **54**, 09MG01 (2015)
27. Katayama, R., Sugiura, S.: Simulation on near-field light generated by a semiconductor ring resonator with a metal nano-antenna for heat-assisted magnetic recording. *Jpn. J. Appl. Phys.* **58**, SKKB01 (2019)
28. Kawazoe, T., Kobayashi, K., Ohtsu, M.: Optical nanofountain: a biomimetic device that concentrates optical energy in a nanometric region. *Appl. Phys. Lett.* **86**, 103102 (2005)
29. Kawazoe, T., Ohtsu, M., Aso, S., Sawado, Y., Hosoda, Y., Yoshizawa, K., Akahane, K., Yamamoto, N., Naruse, M.: Two-dimensional array of room-temperature nanophotonic logic gates using InAs quantum dots in mesa structures. *Appl. Phys. B* **103**, 537 (2011)
30. Katayama, R., Sugiura, S.: Three-dimensional simulation on near-field light generated by semiconductor ring resonator with metal nano-antenna for heat-assisted magnetic recording. *Proc. SPIE* **11125**, 1112506 (2019)
31. Liao, A.S.-H., Wang, S.: Semiconductor injection lasers with a circular resonator. *Appl. Phys. Lett.* **36**, 801 (1980)
32. Krauss, T., Laybourn, P.J.R., Roberts, J.: CW operation of semiconductor ring lasers. *Electron. Lett.* **26**, 2095 (1990)
33. Oku, S., Okayasu, M., Ikeda, M.: Low-threshold CW operation of square-shaped semiconductor ring lasers (orbiter lasers). *IEEE Photonics Technol. Lett.* **3**, 588 (1991)
34. Hohimer, J.P., Craft, D.C., Hadley, G.R., Vawter, G.A., Warren, M.E.: Single-frequency continuous-wave operation of ring resonator diode lasers. *Appl. Phys. Lett.* **59**, 3360 (1991)
35. Chow, C.-M., Bain, J.A.: A split-pole-gapped NFT write head design for transition curvature reduction in heat-assisted magnetic recording. *IEEE Trans. Magn.* **54**, 3001904 (2018)
36. Zienkiewicz, O.C.: *The Finite Element Method*, 3rd edn. McGraw-Hill, London (1977)
37. Chen, Y.-J., Lee, M.-C., Wang, C.-M.: Dielectric function dependence on temperature for Au and Ag. *Jpn. J. Appl. Phys.* **53**, 08MG02 (2014)

Publisher's Note Springer Nature remains neutral with regard to jurisdictional claims in published maps and institutional affiliations.